Biosensing using CNNs to Detect Noisy but Persistent Nanoparticle Binding Events on Supported Lipid Bilayer Systems

Zhen Yuan Yeo [1] **Eun Ho Song** [2] **Kyeongmee Lee** [2] **Jwa-Min Nam** [2] **N. Duane Loh** [3]

[1]*Institute for Digital Molecular Analytics and Science, Nanyang Technological University, Singapore 636921, Singapore* [2]*Department of Chemistry, Seoul National University, Seoul 08826, South Korea* [3]*Department of Physics, National University of Singapore, Singapore 117551, Singapore*. Correspondence to: jmnam@snu.ac.kr, duaneloh@nus.edu.sg.

1. Abstract

We present a novel hybrid U-NET model for biosensing applications that simultaneously performs segmentation and centroid detection of nanoparticles bound to supported lipid bilayer systems. Our approach leverages the full spatial and spectral information in the RGB channels, enabling more accurate detection of extremely noisy but persistent nanoparticle binding events under dark-field illumination. This method surpasses previous single-channel U-NET variants and outperforms state-of-the-art techniques such as T-Rex2 in crowded, low signal-to-noise environments. Implemented in PyTorch and harnessing GPU acceleration, the hybrid U-NET model achieves up to two orders of magnitude speed improvements, making it suitable for high-throughput and real-time on-the-fly analysis. As a first step in a broader diagnostic pipeline, this technique holds promise for detecting rare molecular interactions and mutations (e.g., single-base-pair mismatches or low-abundance proteins) with high sensitivity and specificity.

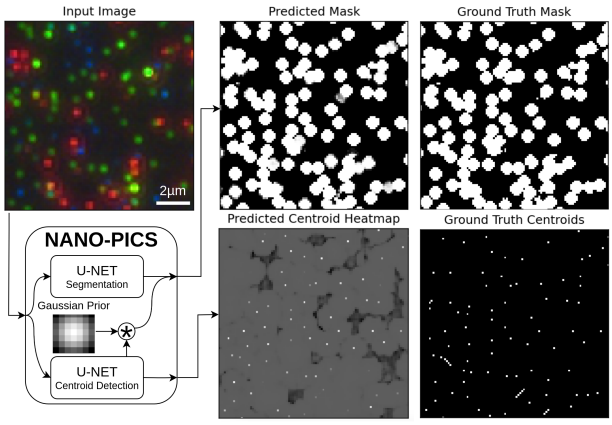

Fig. 1: Schematic of NANOparticle Point spread function-Informed Centroiding and Segmentation (NANO-PICS). NANO-PICS is a hybrid U-NET model that incorporates optical constrains to perform segmentation and centroid detection simultaneously.

2. Introduction

In recent years, there has been growing interest in nanoparticle-based biosensing due to its potential for ultra-sensitive diagnostics in fields ranging from genomics to proteomics [1, 2]. Nanoparticles, functionalized with specialized receptors, can bind to target biomolecules at extraordinarily low concentrations, and does not suffer from photo-bleaching, making them promising labels for single-molecule detection assays [3, 4, 5, 6]. One of the most compelling platforms for these investigations is the supported lipid bilayer (SLB) system, which can be engineered to immobilize nanoparticles in a controlled 2D environment [7, 8, 9, 10]. However, reliably identifying and tracking these nanoparticle binding events is a longstanding challenge, primarily due to the confounding presence of noise and the crowded background signals that are typical in micrographs with a large field-of-view to encompass more particles.

Recent advances in computer vision and artificial intelligence (AI) have significantly pushed the boundaries of image segmentation, particularly through convolutional neural networks (CNNs) such as DeconvNet [11], SegNet [12], and U-NET [13], which deliver state-of-the-art results on everyday objects. Despite these advances, these standard segmentation networks often struggle to accurately segment and localize diffraction-limited micrographs of nanoparticles. This is largely due to their limited exposure to niche image data. For example, electron microscopy images, hyperspectral/multispectral imagery from remote sensing, or tomography scans. Recent methods like T-Rex2 [14], while powerful in sparse environments, have difficulty separating closely spaced or strongly overlapping nanoparticle clusters in noisy data. Our approach directly addresses these limitations by coupling segmentation with centroid detection, facilitated by a Gaussian prior that emphasizes likely nanoparticle locations.

Moreover, for single-molecule biosensing applications that involve nanoparticle detection, obtaining the spatial location of the nanoparticles is crucial for downstream analysis [15, 16, 17]. However, this centroid detection capability is not supported by those CNNs. To address these challenges, we have developed NANOparticle Point spread function-Informed Centroiding and Segmentation (NANO-PICS), a hybrid U-NET model that integrates simultaneous segmentation and centroid detection capabilities while leveraging the color information of multichannel (RGB) microscopy images.

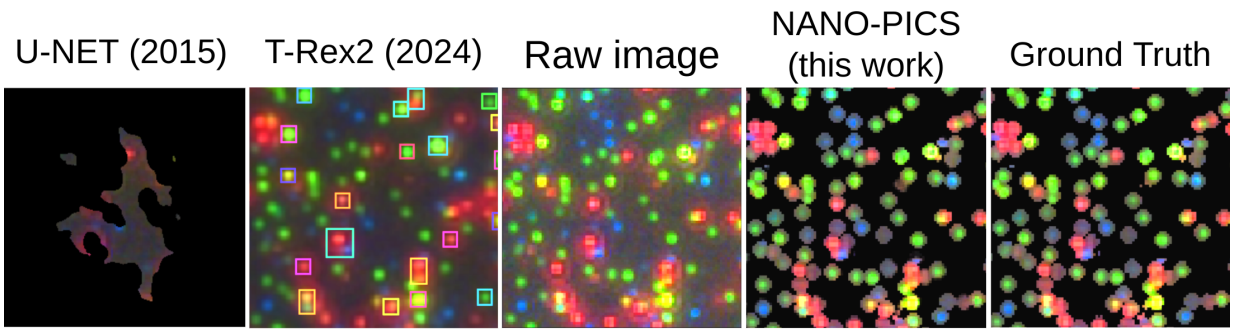

Fig. 2: Comparison with state-of-the-art segmentation architectures. Previous segmentation models like U-NET and T-Rex2 are unable to satisfactorily segment dark-field images of nanoparticles. The crowded and noisy environment of the images causes these models to perform poorly. The ground truth segmentation was obtained by aggregating masks from manually determined thresholds of raw images, described in Figure A2.

3. Discussion

The key novelty of NANO-PICS is summarized in the following paragraphs.

Improved multi-channel analysis: Conventional single-channel approaches to localization (for example, in fluorescence microscopy), does not utilize the valuable spectral information carried in the RGB channels, leading to reduced accuracy. Moreover, the dynamic range of signals in fluorescence microscopy can vary significantly across channels, providing essential clues for disambiguating nanoparticle binding events from background noise. The proposed NANO-PICS solves this by operating simultaneously on all three channels.

Simultaneous segmentation and centroid detection: The combined information of segmentation and centroid detection is incorporated in the loss function of the model. This allows for a single model to perform two tasks simultaneously. This reduces the need for other ad-hoc image processing steps.

PSF-informed segmentation The dual-design that explicitly separates segmentation from centroid detection allows each network head to learn specialized features, one focusing on object boundary delineation and the other on localizing the brightest point of interest. The point-spread function (PSF) prior, in this case, a Gaussian profile, further refines centroid predictions, a critical step when signals are faint or overlapping, and standard neural networks tend to blur or over-segment.

High-throughput imaging capability: High sensitivity biosensing applications require analyzing large volumes of data quickly, to detect and sift statistically important signals, whether for real-time diagnostics or high-throughput screening. The PyTorch implementation of our NANO-PICS allows seamless GPU acceleration, delivering speed-ups of up to 10x–100x compared to CPU-based or less optimized pipelines. Such performance gains are needed for "on-the-fly" analysis, enabling timely decision-making in clinical or laboratory settings.

4. Conclusion

This study demonstrates that simultaneously segmenting and detecting nanoparticle centroids in noisy, multichannel microscopy images of supported lipid bilayer systems is both feasible and advantageous. By leveraging the hybrid U-NET architecture, one can achieve robust, high-throughput performance that outstrips both classic single-channel U-NET variants and more modern, but less specialized methods like T-Rex2. The deployment-ready PyTorch implementation offers immediate benefits for large-scale experiments or point-of-care diagnostics.

In the broader context of biosensing and medical diagnostics, this represents a key first step in a pipeline aimed at ultra-sensitive detection tasks, such as identifying single-base-pair mismatches in nucleic acids [7, 15] or capturing trace concentrations of proteins of diseases markers [18]. The improved fidelity and throughput of the model pave the way for subsequent analytical stages—e.g., advanced classification, quantitative measurements of binding kinetics, or multiplexed assays—where precise localization and segmentation of nanoparticles are foundational. As the field shifts toward ever more sensitive, low-volume biosensing techniques, this hybrid U-NET approach stands poised to enable rapid, accurate, and cost-effective diagnostic workflows.

Acknowledgments

The authors gratefully acknowledge the National University of Singapore (NUS), Institute for Digital Molecular Analytics and Science (IDMxS) and the Bio&Medical Technology Development Program of the National Research Foundation (NRF) funded by the Korean government (MSIT) (No. RS-2023-00222838).

References

[1] Manickam Ramesh, Ravichandran Janani, Chinnaiyan Deepa, and Lakshminarasimhan

Rajeshkumar. Nanotechnology-enabled biosensors: A review of fundamentals, design principles, materials, and applications. *Biosensors (Basel)*, 13(1):40, December 2022.

[2] Sumit Malik, Joginder Singh, Rohit Goyat, Yajvinder Saharan, Vivek Chaudhry, Ahmad Umar, Ahmed A Ibrahim, Sheikh Akbar, Sadia Ameen, and Sotirios Baskoutas. Nanomaterials-based biosensor and their applications: A review. *Heliyon*, 9(9):e19929, September 2023.

[3] Wei Tang, Dingzhong Wang, Yi Xu, Na Li, and Feng Liu. A self-assembled DNA nanostructure-amplified quartz crystal microbalance with dissipation biosensing platform for nucleic acids. *Chem. Commun. (Camb.)*, 48(53):6678–6680, July 2012.

[4] Peng He, Lijun Liu, Wenping Qiao, and Shusheng Zhang. Ultrasensitive detection of thrombin using surface plasmon resonance and quartz crystal microbalance sensors by aptamer-based rolling circle amplification and nanoparticle signal enhancement. *Chem. Commun. (Camb.)*, 50(12):1481–1484, February 2014.

[5] Shubham Arunrao Chinchulkar, Paloma Patra, Dheeraj Dehariya, Tejaswini Appidi, and Aravind Kumar Rengan. Gold nanoparticle–based biosensing applications and fundamentals of sensor technology: principles and novel designs. In *Fundamentals of Sensor Technology*, pages 669–723. Elsevier, January 2023.

[6] Swayandipta Dey, Mathias Dolci, and Peter Zijlstra. Single-molecule optical biosensing: Recent advances and future challenges. *ACS Phys. Chem. Au*, 3(2):143–156, March 2023.

[7] Young Kwang Lee, Sungi Kim, Jeong-Wook Oh, and Jwa-Min Nam. Massively parallel and highly quantitative single-particle analysis on interactions between nanoparticles on supported lipid bilayer. *J. Am. Chem. Soc.*, 136(10):4081–4088, March 2014.

[8] Kevin L Hartman, Sungi Kim, Keunsuk Kim, and Jwa-Min Nam. Supported lipid bilayers as dynamic platforms for tethered particles. *Nanoscale*, 7(1):66–76, January 2015.

[9] Keunsuk Kim, Jeong-Wook Oh, Young Kwang Lee, Jiwoong Son, and Jwa-Min Nam. Associating and dissociating nanodimer analysis for quantifying ultrasmall amounts of DNA. *Angew. Chem. Int. Ed Engl.*, 56(33):9877–9880, August 2017.

[10] So Young Choi, Young Suk Yu, Eunhye Park, Sung Hee Baek, and Jwa-Min Nam. Cell-interface-deciphering lipid nanotablet for nanoparticle logic gate-based real-time single-cell analysis. *Nano Lett.*, 25(7):2725–2731, February 2025.

[11] Hyeonwoo Noh, Seunghoon Hong, and Bohyung Han. Learning deconvolution network for semantic segmentation. *arXiv [cs.CV]*, May 2015.

[12] Vijay Badrinarayanan, Alex Kendall, and Roberto Cipolla. SegNet: A deep convolutional encoder-decoder architecture for image segmentation. *arXiv [cs.CV]*, November 2015.

[13] Olaf Ronneberger, Philipp Fischer, and Thomas Brox. U-net: Convolutional networks for biomedical image segmentation. In *Lecture Notes in Computer Science*, Lecture notes in computer science, pages 234–241. Springer International Publishing, Cham, 2015.

[14] Qing Jiang, Feng Li, Zhaoyang Zeng, Tianhe Ren, Shilong Liu, and Lei Zhang. T-Rex2: Towards generic object detection via text-visual prompt synergy. *arXiv [cs.CV]*, March 2024.

[15] Sungi Kim, Jeong-Eun Park, Woosung Hwang, Jinyoung Seo, Young-Kwang Lee, Jae-Ho Hwang, and Jwa-Min Nam. Optokinetically encoded nanoprobe-based multiplexing strategy for MicroRNA profiling. *J. Am. Chem. Soc.*, 139(9):3558–3566, March 2017.

[16] Jinyoung Seo, Sungi Kim, Ha H Park, Da Yeon Choi, and Jwa-Min Nam. Nano-bio-computing lipid nanotablet. *Sci. Adv.*, 5(2):eaau2124, February 2019.

[17] Sungi Kim, Namjun Kim, Jinyoung Seo, Jeong-Eun Park, Eun Ho Song, So Young Choi, Ji Eun Kim, Seungsang Cha, Ha H Park, and Jwa-Min Nam. Nanoparticle-based computing architecture for nanoparticle neural networks. *Sci. Adv.*, 6(35):eabb3348, August 2020.

[18] Dimitra G Georganopoulou, Lei Chang, Jwa-Min Nam, C Shad Thaxton, Elliott J Mufson, William L Klein, and Chad A Mirkin. Nanoparticle-based detection in cerebral spinal fluid of a soluble pathogenic biomarker for alzheimer's disease. *Proc. Natl. Acad. Sci. U. S. A.*, 102(7):2273–2276, February 2005.

Appendix A. Methods

1.1 Data Acquisition and Preparation

Nanoparticle synthesis: Nanoparticles for the red signal are gold nanorods synthesized by a seed-mediated growth mechanism. Nanoparticles for the green signal are spherical gold nanoparticles (50 nm) purchased from BBI Solutions (Cardiff, UK). Nanoparticles for the blue signal are gold-silver core-shell nanoparticles synthesized by a core-shell growth mechanism. The spectral response and other characterization are described in [15]. Microscopy Setup: We captured images of nanoparticles bound to supported lipid bilayers under dark-field conditions. The data consisted of images with three channels corresponding to red, green, and blue emissions. Preprocessing: Images were normalized to reduce channel-to-channel intensity variations.

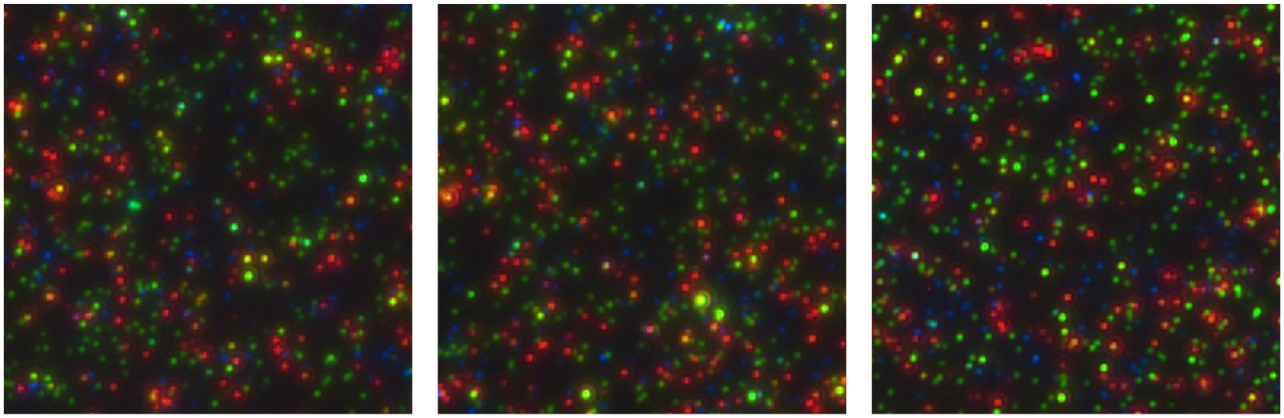

Fig. A1: Samples of input data used. A total of 1120 frames of 256 pixels by 256 pixels were used.

1.2 Model Architecture: NANO-PICS

Segmentation U-NET: Trained to produce a soft mask that differentiates nanoparticles from background. Centroid Detection U-NET: Generates a heatmap capturing the most probable locations of nanoparticle centroids, using a Gaussian prior as additional training signal. Gaussian Prior Enhancement: The centroid detection U-NET outputs a heatmap, which is convolved (element-wise multiplied) with a precomputed 2D Gaussian kernel prior. This prior emphasizes Gaussian-like structures corresponding to nanoparticles in each color channel, effectively guiding the training toward accurate localization even under high noise.

1.3 Loss Function

For segmentation, binary cross-entropy loss was employed. For centroid detection, mean squared error (MSE) and a sparsity metric was used to promote small, high-intensity regions corresponding to centroids. The full loss function is shown in Appendix C. Implementation: The model was built using PyTorch, leveraging GPU acceleration (NVIDIA GTX 1080).

1.4 Segmentation Performance

Quantified using intersection over union (IoU) and the F1 score to evaluate how closely the predicted mask matches the ground truth. Centroid Detection Accuracy: Computed via the precision and recall of predicted centroid locations (within a fixed radius of the ground-truth positions), as well as the mean Euclidean distance between predicted and true centroids. Speed Benchmarking: Execution times were recorded for CPU-only vs. GPU-accelerated runs across a range of image sizes and batch configurations.

Appendix B. Obtaining ground truth segmentation

Ground truth segmentation was performed by manually adjusting a threshold level for each color channel in the images, shown in Figure A2. This step helps ensure that brighter nanoparticle signals are separated from the background. However, setting the threshold too high can unintentionally exclude dimmer particles, leading to an undercount. Conversely, setting it too low may include noise or non-nanoparticle structures. As a result, each color channel demands its own careful tuning so that the segmentation captures as many particles as possible while minimizing false positives. This manual process can be labor-intensive and prone to variability, particularly when dealing with multiple channels and different imaging conditions.

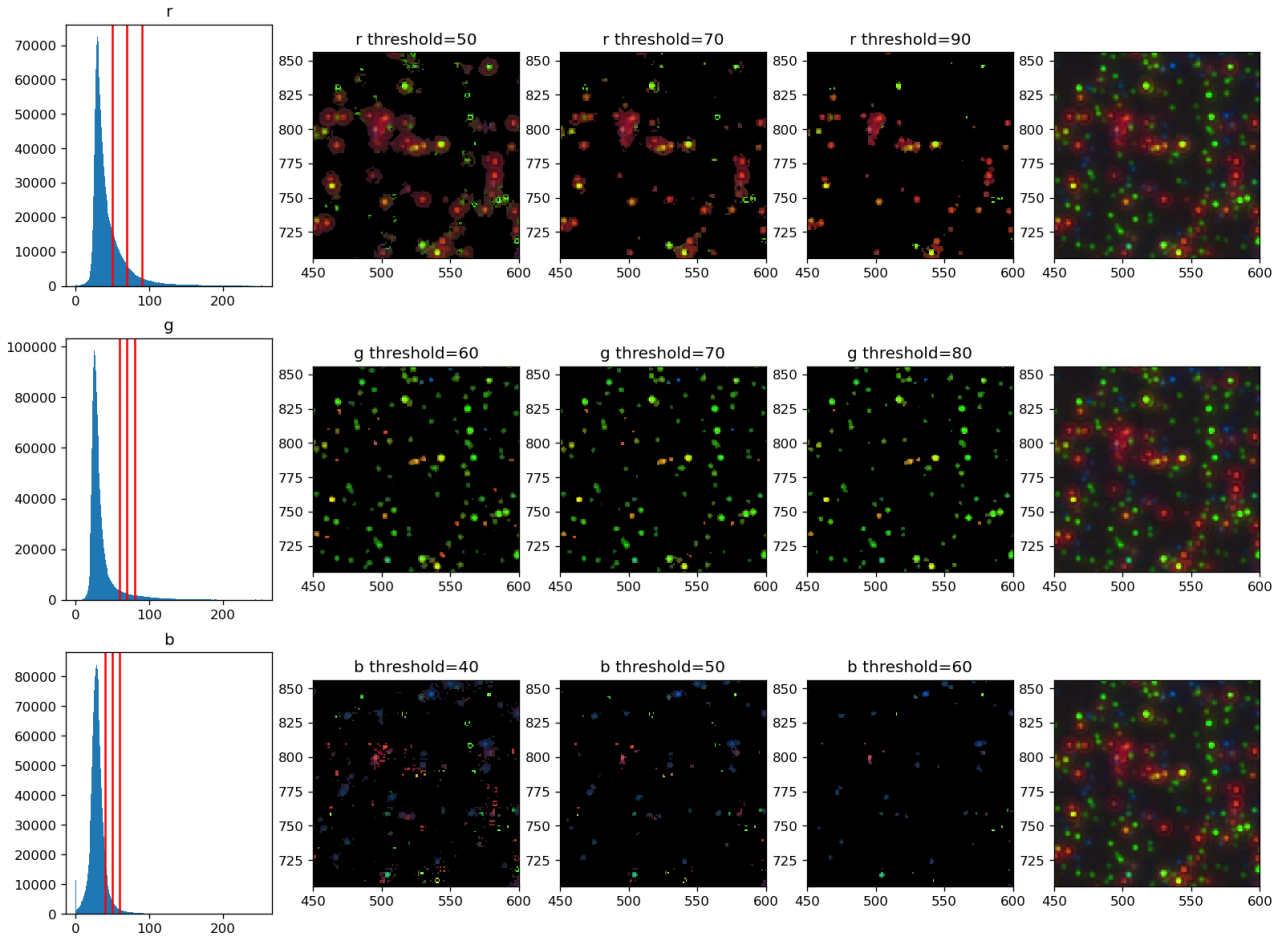

Fig. A2: Ground truth segmentation was determined by manual determination of threshold level for each color channel. At higher threshold levels, dimmer particles are excluded. Manual tuning for each channel is required to capture as many particles as possible.

Appendix C. Loss function of NANO-PICS

The loss function of NANO-PICS consist of two major parts. One from the segmentation and one from the centroiding.

$$\mathcal{L}_{\text{total}} = \mathcal{L}_{\text{seg}} + \mathcal{L}_{\text{centroid}}, \tag{A1}$$

where $\mathcal{L}_{\text{seg}}$ is the segmentation loss and $\mathcal{L}_{\text{centroid}}$ is the centroid loss.

3.1 Segmentation loss

The segmentation loss is simply the Binary Cross-Entropy loss,

$$\mathcal{L}_{\text{seg}} = \text{BCE}(S_{\text{pred}}, S_{\text{target}}), \tag{A2}$$

where S_{pred} is the predicted segmentation and S_{target} is the target segmentation.

3.2 Centroiding loss

The centroiding loss can be further broken down into two components. One from the determination of peaks and one novel component (in this work) that relates to the "shape" of the nanoparticle.

$$\mathcal{L}_{\text{centroid}} = \mathcal{L}_{\text{peaks}} + \mathcal{L}_{\text{Gaussian}} \tag{A3}$$

$$\mathcal{L}_{\text{peaks}} = \frac{1}{B}\sum_{i=1}^{B}\left(\frac{1}{|P^i_{\text{out}}|}\sum_{p\in P^i_{\text{out}}}\min_{q\in P^i_{\text{targ}}}\|p-q\|_2 + \text{BCE}(C^i_{\text{pred}}, C^i_{\text{target}}) + \mathcal{R}^i_{\text{sparsity}}\right), \tag{A4}$$

where B is the batch size, P^i_{out} is the set of peak positions in the i-th predicted centroid map, P^i_{targ} is the set of peak positions in the i-th target centroid map, C^i_{pred} is the i-th predicted centroid map, C^i_{target} is the i-th target centroid map and $\mathcal{R}^i_{\text{sparsity}}$ is the sparsity regularization term.

$$\mathcal{R}^i_{\text{sparsity}} = \begin{cases} \frac{|P^i_{\text{out}}|}{|P^i_{\text{targ}}|}, & \text{if } |P^i_{\text{out}}| > |P^i_{\text{targ}}| \text{ and } |P^i_{\text{targ}}| \neq 0 \\ \frac{|P^i_{\text{targ}}|}{|P^i_{\text{out}}|}, & \text{if } |P^i_{\text{targ}}| > |P^i_{\text{out}}| \text{ and } |P^i_{\text{out}}| \neq 0 \\ 1, & \text{otherwise} \end{cases}, \tag{A5}$$

This sparsity term penalizes the model if there is a difference between the number of predicted peaks and the number of ground truth peaks.

$$\mathcal{L}_{\text{Gaussian}} = \frac{1}{B}\sum_{i=1}^{B}\frac{1}{H\times W}\sum_{h=1}^{H}\sum_{w=1}^{W}\text{BCE}((G * C^i_{\text{pred}})_{h,w}, S^i_{\text{target}_{h,w}}), \tag{A6}$$

where G is the Gaussian kernel: $G(x,y) = \frac{1}{2\pi\sigma^2}e^{-\frac{x^2+y^2}{2\sigma^2}}$, $*$ denotes the convolution operation, H and W are the height and width of the feature maps. This Gaussian loss provides an additional constraint between the predicted peaks and the segmentation model.

Appendix D. CNN architectures

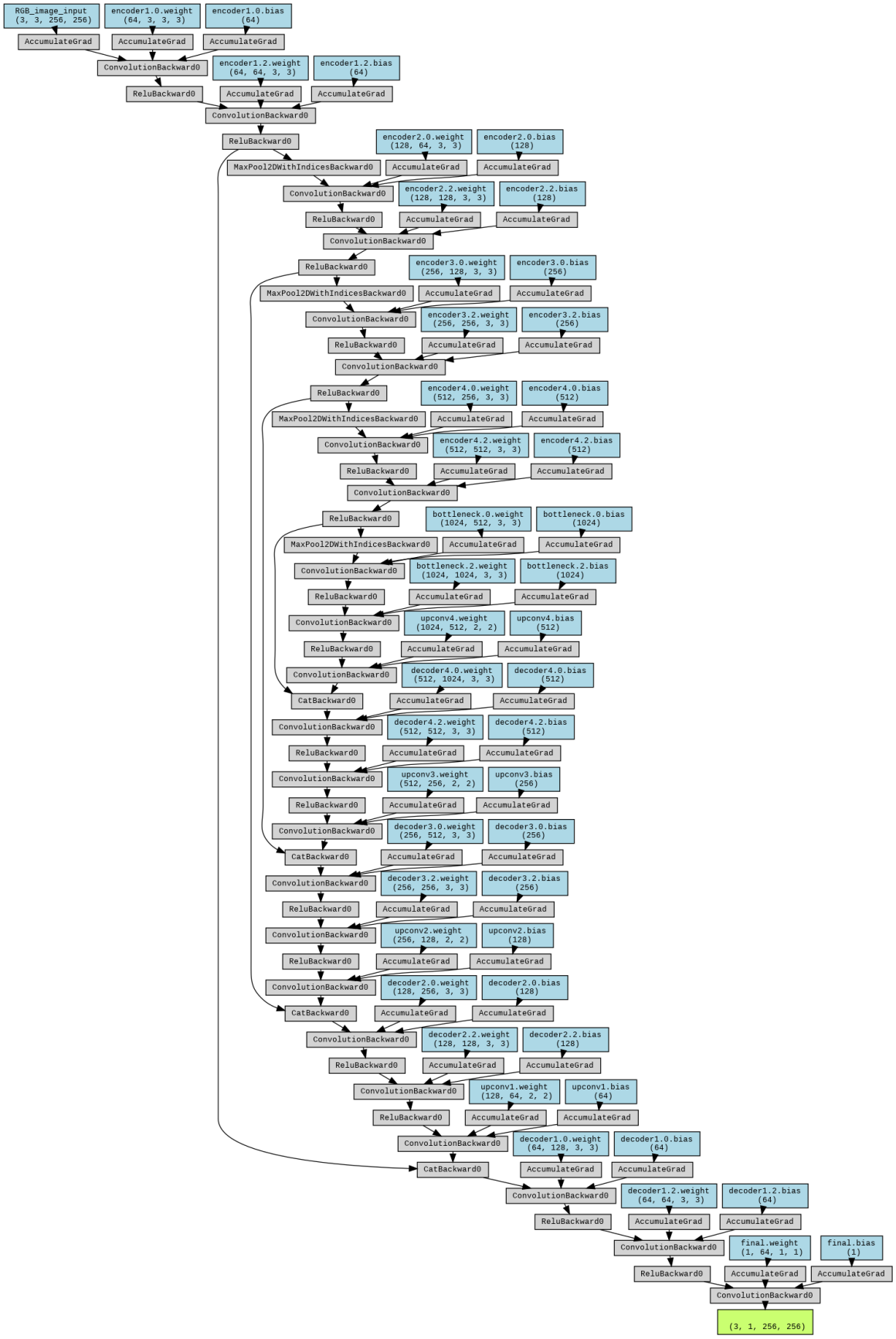

Fig. A3: Basic U-NET architecture inspired from [13]. Here, 256x256 pixels input were used instead of the original 128x128 pixels.

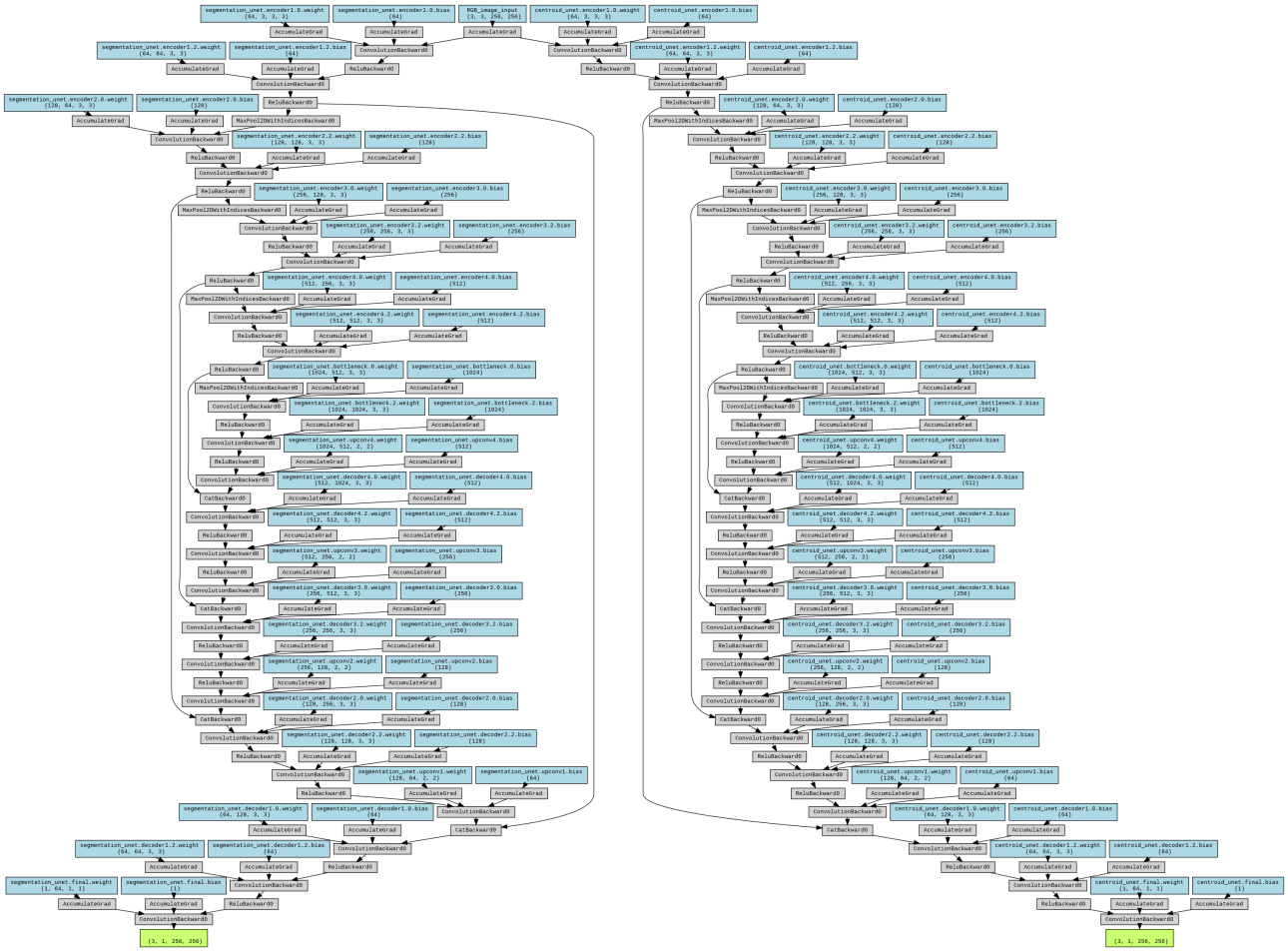

Fig. A4: NANO-PICS architecture. NANO-PICS is a hybrid of two U-NETs. The left arm was trained for segmentation, while the right arm was trained for centroiding.